

Electronic Supplementary Information (ESI)

Sulfonated dendritic mesoporous silica nanospheres: a metal-free Lewis acid catalyst for the upgrading of carbohydrates

Erlen Y. C. Jorge,^{a,b} Carolina G. S. Lima,^{a,c*} Thiago M. Lima,^{a,c} Lucas Marchini,^a Manoj B. Gawande,^d Ondřej Tomanec,^d Rajender S. Varma^{d*} and Marcio W. Paixão^{a*}

^aCentre of Excellence for Research in Sustainable Chemistry (CERSusChem), Department of Chemistry, Federal University of São Carlos – UFSCar, Rodovia Washington Luís, km 235 - SP-310, São Carlos, São Paulo, 13565-905, Brazil.

^bUniversity of Havana, Institute of Science and Technology of Materials, Zapata and G, Centro Habana, Havana 10400, Cuba.

^cInstitute of Chemistry, Fluminense Federal University, Outeiro São João Batista, Niterói, Rio de Janeiro, Brazil-24020-150.

^dRegional Centre of Advanced Technologies and Materials, Departments of Physical Chemistry Faculty of Science, Palacky University, Šlechtitelů 27, 783 71 Olomouc, Czech Republic.

Contents:

1. General methods.....	S1
2. Experimental procedures for the synthesis of the silica materials.....	S3
3. Additional characterization of DMSi and DMSi-SA.....	S5
4. Characterization of the DMSi-SA catalyst after the recyclability studies.....	S9
5. Additional characterization of the silica materials: HRTEM, EDS, N ₂ physisorption, XPS and Pyr-FTIR.....	S10
6. Discussion on the characterization and catalytic evaluation of different sulfonic acid-functionalized silica materials.....	S24
7. Additional chromatographic data used for the quantification of the products.....	S26
8. References.....	S30

1. General methods

The particle size and morphological studies of the DMSi support and the DMSi-SA catalyst were performed by TEM (Transmission Electron Microscopy). The TEM analyses were conducted using JEOL JEM 2010F at 160kV of accelerating voltage.

Microscopic images were obtained for all sulfonated catalysts by HRTEM TITAN 60-300 with X-FEG type emission gun, operating at 80 kV; this microscope is equipped with a Cs image corrector and a STEM high-angle annular dark-field detector (HAADF). The point resolution is 0.06 nm in HRTEM mode. The elemental mappings were obtained by STEM-Energy Dispersive X-ray Spectroscopy (EDS) with an acquisition time of 20 min. For HRTEM analyses, the powder samples were dispersed in ethanol and ultrasonicated for 5 min. One drop of this solution was placed on a copper grid with a holey carbon film. The sample was then dried at room temperature.

Low angle x-ray diffraction patterns were recorded with a PANalytical X'Pert PRO MPD (PANalytical, Netherlands) diffractometer in the Bragg-Brentano geometry, Co-K α radiation (40 kV, 30 mA, $\lambda = 0.1789$ nm) equipped with an X'Celerator detector and programmable divergence and diffracted beam anti-scatter slits. The measurement range was $2\theta: 0^\circ - 5^\circ$ with a step size of 0.017° .

The nitrogen desorption analyses were conducted at a Micromeritics equipment (ASP-2420). The samples were treated under vacuum at 200 °C for 240 minutes for the elimination of water and physically adsorbed gases. Then, the samples were transferred to the adsorption unit, where liquid nitrogen is fed to the sample at varying relative pressures (p/p_0).

The infrared spectrum of adsorbed pyridine was recorded on a Bruker Fourier Transform Infrared spectrophotometer model Vertex-70. For the qualitative acidity determination, the samples were previously heated at 250 °C for 2h under nitrogen flow (100 mL min^{-1}). The application of pyridine over the samples was conducted using a pyridine/nitrogen flow (30 mL min^{-1}) at 150 °C for 10 min. Next, the N₂ flow was kept constant (100 mL min^{-1}) at 200 °C for 1 h for the removal of the physically adsorbed pyridine. The materials were then analyzed by DRIFTS in the 1800-1400 cm^{-1} wavenumber range using a spectral resolution of 4 cm^{-1} with the collection of 32 scans for each spectrum.

The infrared spectrum of adsorbed pyridine was recorded on a Fourier Transform Infrared spectrophotometer model Prestigi-21 in the range of 1800–1400 cm^{-1} wavenumber. For the qualitative acidity determination, 50 mg of sample were subjected to a heat treatment in a tubular furnace at 300 °C and 100 mL min^{-1} N_2 flow for 1 h. Gaseous pyridine was then adsorbed on the samples for 1 h at 150 °C with a N_2 gas carrier flow at 100 mL min^{-1} . Next, the N_2 flow was kept constant for 1 h at 150 °C for the removal of the physically adsorbed pyridine.

XPS surface investigation has been performed on the PHI 5000 VersaProbe II XPS system (Physical Electronics) with monochromatic Al-K α source (15 kV, 50 W) with photon energy of 1486.7 eV. Dual beam charge compensation was used for all measurements. All the spectra were measured in the vacuum of 1.4×10^{-7} Pa and at the room temperature of 22 °C. For the high-resolution spectra was the pass energy set up to 23.500 eV and step size 0.200 eV. The spectra were evaluated with the MultiPak (Ulvac - PHI, Inc.) software. All binding energy (BE) values were referenced to the C1s peak at 284.80 eV.

The total acidity of the samples was determined by aqueous titration using thymol blue as indicator. The samples were previously submitted to an ionic exchange with KCl and the resulting HCl was titrated with a NaOH solution previously standardized using potassium hydrogen phthalate ($\text{KHC}_8\text{H}_4\text{O}_4$). All analyses were performed as triplicates and with different batches of the materials.

Thermogravimetric analyses (TGA) of the DMSi catalyst were performed in air atmosphere at a heating rate of 10 °C min^{-1} using an STA 449 C Jupiter analyzer (Netzsch).

The yield of the reactions was determined using GC-MS with 4-nitrophenol as an internal standard. Calibration curves were acquired in triplicates for each of the expected products. The samples were analyzed using Shimadzu GCMS-QP2010S Gas Chromatograph coupled to a MS detector equipped with an ZB-5MS column (30 m x 0.25 mm x 0.25 μm) under the operation parameters: temperature of inlet of 250 °C, temperature ramp of the oven from 100 to 250 °C at a rate of 10 °C min^{-1} .

2. Experimental procedures for the synthesis and functionalization of the silica materials

2.1 Synthesis of the mesoporous silica KCC-1 material. The KCC-1 silica was synthesized following a procedure described by Yu and co-workers.^[1] A solution containing 0.5 g of hexadecylpyridinium bromide (CPB), 0.75 mL of *n*-pentanol and 15 mL of cyclohexane was added to a mixture of 0.3 g of urea and 15 mL of water under stirring at room temperature. Then, 1.25 mL of tetraethyl orthosilicate (TEOS) were added and the mixture was transferred to a 50 mL Teflon-lined autoclave and heated at for 4 h in an oven at 120 °C. The obtained material was washed with ethanol and dried at 60 °C for 12 h. Finally, the material was calcined at 550 °C for 5 h.

2.2 Synthesis of the mesoporous silica MCM-41 material. The MCM-41 was synthesized following a procedure described by Grün and co-workers.^[2] A solution containing 13.2 g of aqueous ammonia (32 wt.%) and 60.0 g of absolute ethanol was added to a solution containing 2.5 g of *n*-hexadecyltrimethylammonium bromide (CTAB) dissolved in 50 mL of deionized water. The solution was stirred for 15 min at 250 rpm and, subsequently, 4.7 g of TEOS were added. The mixture was then stirred for 2 h. The resulting material was filtered and washed with distilled water and methanol several times. Next, the white powder was dried at 60 °C for 24 h followed by trituration and calcination at 550 °C in air atmosphere for 5 h.

2.3 Synthesis of large-pore silica FDU-12 material. The FDU-12 silica was synthesized following a procedure described by Kruk and co-workers with some modification.^[3] A solution containing 3.0 g of Pluronic F127 copolymer and 185 mL of HCl 1.97 M was placed in a water bath set to 15 °C and stirred until total homogenization. Then, 4.7 mL of *p*-cymene and 15.0 g of KCl were added to the mixture. After 2 h of constant stirring, 13.3 mL of TEOS were added and the mixture was stirred for 24 h in an open container at 15 °C. Next, the reaction mixture was refluxed at 100 °C for 24 h. The sample was recovered by filtration without washing and left to dry in the air. Then, the dried as-synthesized material was subjected to an additional hydrothermal treatment in an acidic solution; 0.5 g of the as-synthesized sample were added to 30 mL of a HCl 1.97 M solution and heated at 100 °C in a Teflon-lined autoclave for 24 h. The resultant material was cooled to room temperature and filtered, followed by washing with distilled water several times. Next, the white powder

was dried at 60 °C for 24 h, followed by trituration and calcination at 550 °C in air atmosphere for 5 h.

2.4 Synthesis of spherical silica particles by Stöber process. The Stöber silica was synthesized following a procedure described by Wang and co-workers with some modification.^[4] First, 10.8 mL of deionized water, 9.8 mL of concentrated ammonia and 73.8 mL of ethanol were mixed for 10 min, followed by the addition of 5.6 mL of TEOS and magnetic stirring for 12 h at room temperature. The resulting material was cooled to room temperature and centrifuged at 5000 rpm for 15 min, followed by washing with water and ethanol several times. Then, the white powder was dried at 150 °C for 5 h.

2.5 Synthesis of microporous silica silicalite-1. The silicalite used as support for the catalyst was synthesized following a procedure described by Zhou and co-workers.^[5] A solution containing 11.16 mL of TEOS, 27 mL of water and 3 mL of tetrapropylammonium hydroxide (TPAOH, 40 wt% aqueous solution) was stirred for 24 h at room temperature. Then a solution containing 0.08 g of NaOH, 27 mL of water and 3 mL of TPAOH was added, and the resulting mixture was stirred for 2 h at room temperature. The solution was then transferred to a 50 mL Teflon-lined autoclave, which was kept under stirring and heating at 150 °C in a sand bath for 24 h. Then, the white material was washed with water several times and dried at 60 °C for 24 h, followed by trituration and calcination at 500 °C in air atmosphere for 16 h.

2.6 Synthesis of SBA-15. The SBA-15 silica was synthesized following a procedure described by Zhao and co-workers.^[1] 4 g of Pluronic P123 were dissolved in 30 mL of distilled water at 50 °C. Then, 120 mL of a HCl 2.0 mol L⁻¹ solution were added to the mixture, which was stirred at 50 °C for 30 min. Next, 10 mL of TEOS were added and the mixture was refluxed at 50 °C for 24 h under constant stirring. Then, the mixture was refluxed at 80 °C for 24 h under static conditions. The resulting white powder was washed with water several times and dried at 60 °C for 24 h, followed by trituration and calcination at 550 °C in air atmosphere for 5 h.

2.7 Functionalization of the silica materials with sulfonic acid. After synthesized and fully characterized, the silica materials were functionalized with sulfonic acid groups using the same procedure used for the DMSi nanospheres.^[6] 1 g of the as-prepared silica

material were added to a solution containing 30 mL of distilled water and 200 mg of sodium chloride under vigorous stirring at room temperature for 30 min. Then, 1 mL of 3-mercaptopropyl trimethoxysilane (MPTMS) was added to the mixture, which was refluxed at 100 °C under magnetic stirring (600 rpm) for 24 h. The mercaptopropyl functionalized material was filtered under vacuum and washed several times with distilled water, followed by drying at 50 °C under vacuum overnight. The thiol groups were then converted into sulfonic acid groups by a mild oxidation process using hydrogen peroxide as oxidant. For this step, the dried and triturated DMSi-MP material (~1.6 g) was added into 30 mL of a 30% hydrogen peroxide solution and vigorously stirred (1000 rpm) at room temperature for 24 h. The resultant material was filtered under vacuum and washed several times with methanol, followed by drying at 50 °C under vacuum for 24 h. The sulfonic acid-functionalized silica materials were named as Silica-SA.

3. Additional characterization of the DMSi support and the DMSi-SA catalyst

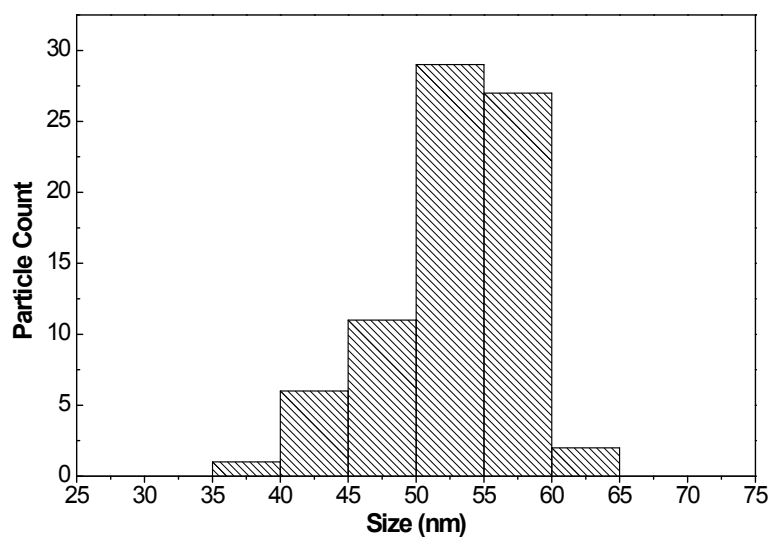


Figure S1. Particle count for the DMSi nanospheres used as support. The TEM image used in the particle count is depicted in the manuscript as Figure 1a.

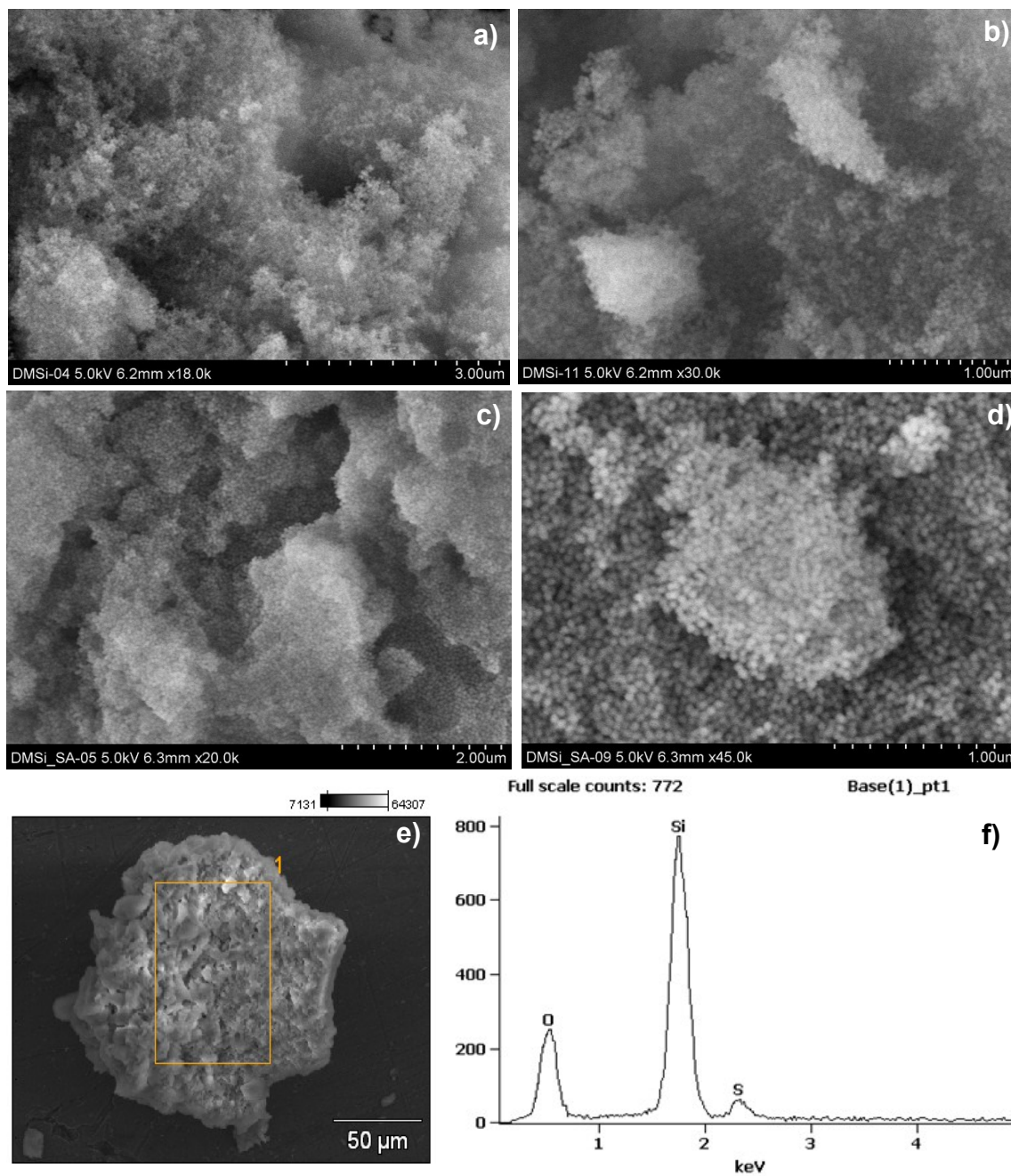


Figure S2. SEM images of a) and b) the DMSi support, c) and d) the DMSi-SA catalyst and e) SEM image depicting the area in which were conducted the F) EDS analysis.

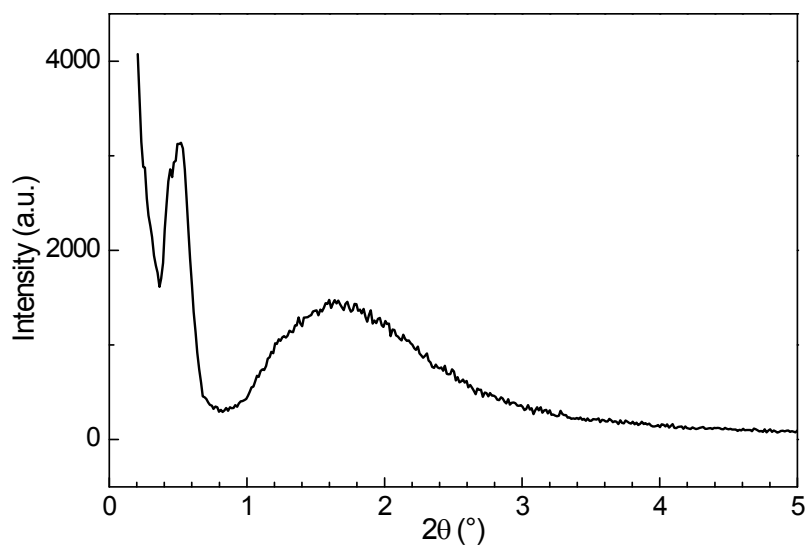


Figure S3. Low angle X-ray diffractogram of the DMSi nanospheres.

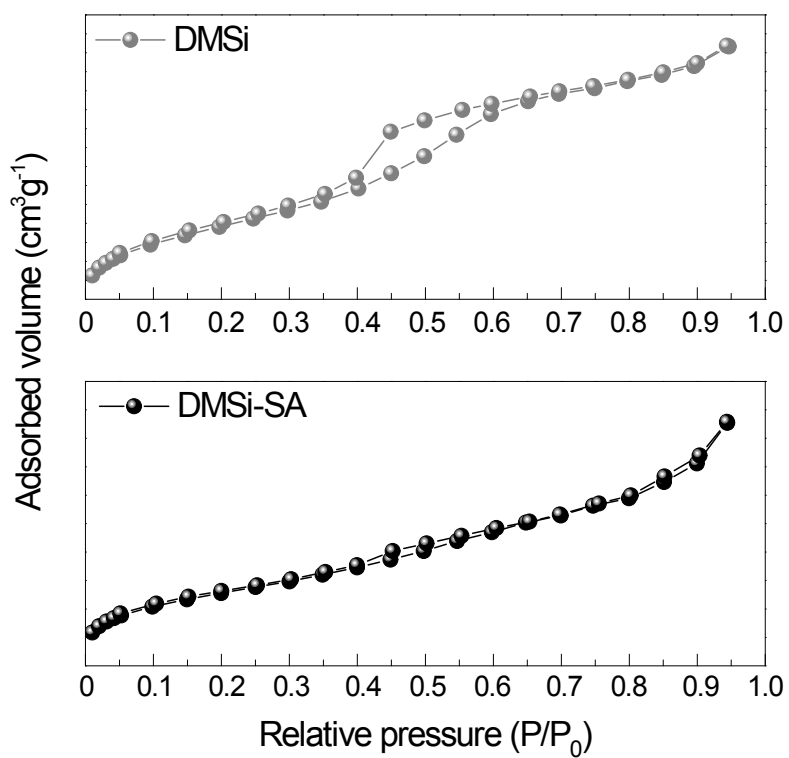


Figure S4. Nitrogen adsorption/desorption isotherms of DMSi and DMSi-SA.

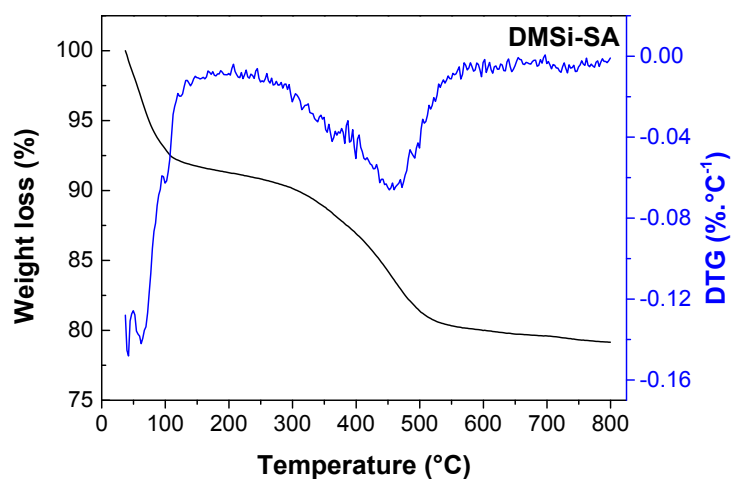


Figure S5. TG and DTG curves for the DMSi-SA sample.

The TG and DTG curves of DMSi-SA (Figure S5) show a weight loss in the range of 50 °C to 150 °C (~7.5%), which is attributed to the desorption of water molecules, as well as a pronounced weight loss between 240 °C and 600 °C (~ 15%), a consequence of the thermal decomposition of the sulfonic acid groups. Similar results had already been observed for other types of sulfonic acid-functionalized silica materials.^[7]

4. Characterization of the DMSi-SA catalyst after the recyclability studies

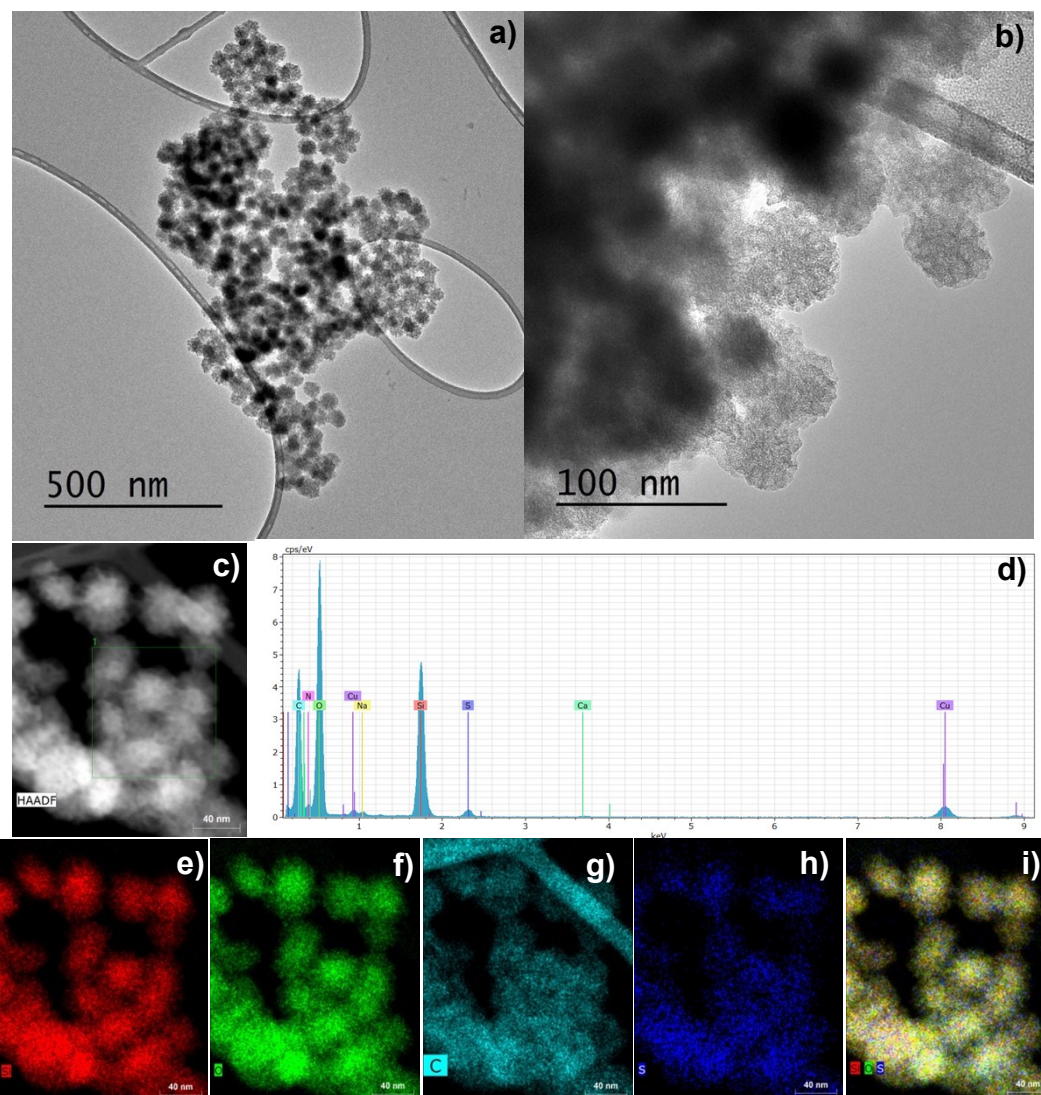


Figure S6. a) and b) HRTEM images, c) high-angle annular dark-field (HAADF) STEM image, d) EDS spectrum of the delimited area in Figure S21c and e) Si, f) O, g) C, h) S and i) Si, O and S elemental chemical mapping for the DMSi-SA catalyst after the recyclability studies. Scale bar: a) 500 nm, b) 100 nm, c and e-i) 40 nm.

5. Additional characterization of the silica materials

5.1 Morphological and elemental characterization of the sulfonated KCC-1 silica catalyst (KCC-1-SA).

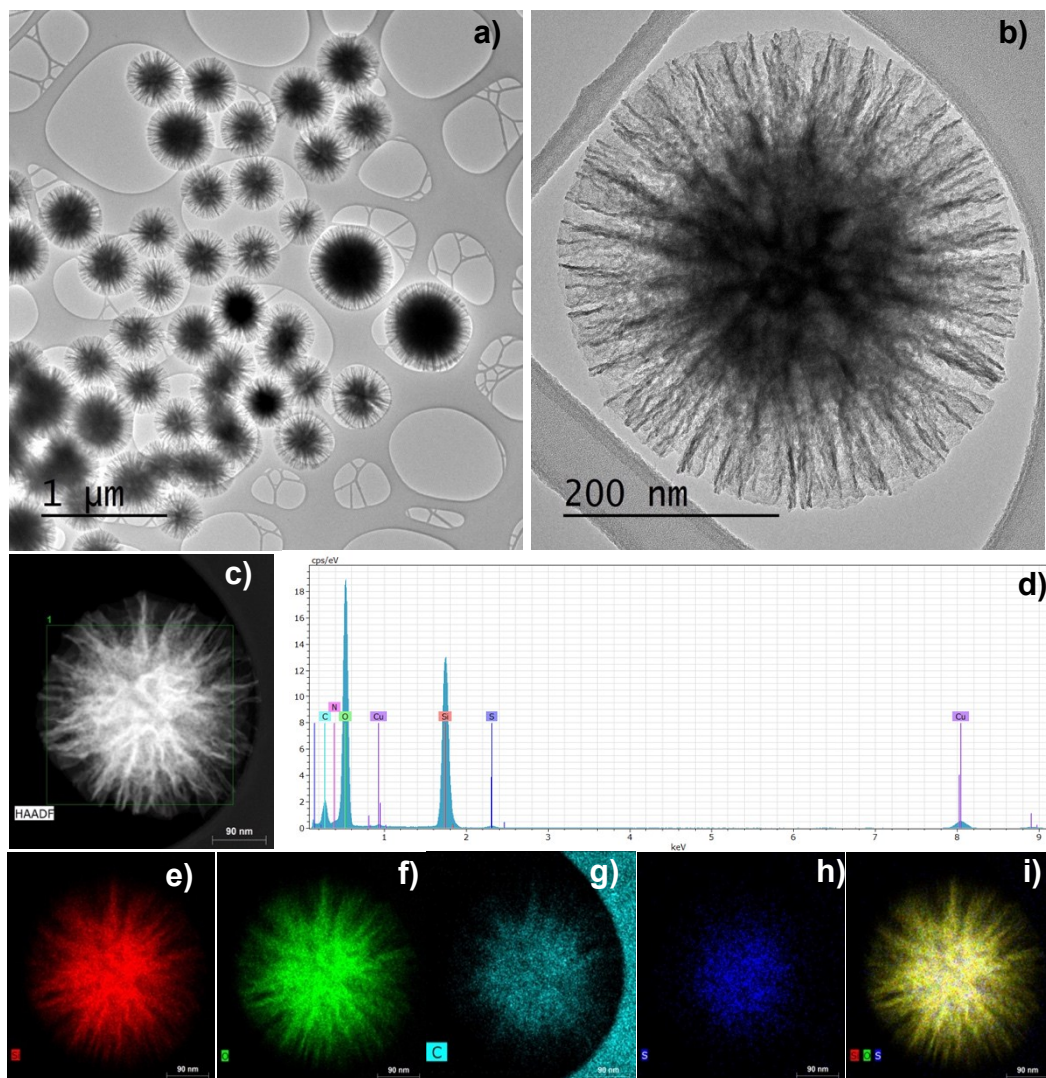


Figure S7. a) and b) HRTEM images, c) high-angle annular dark-field (HAADF) STEM image, d) EDS spectrum of the delimited area in Figure S1c and e) Si, f) O, g) C, h) S and i) Si, O and S elemental chemical mapping for the KCC-1-SA catalyst. Scale bar: a) 1 μm , b) 200 nm and c, e-i) 90 nm.

5.2 Morphological and elemental characterization of the sulfonated MCM-41 silica catalyst (MCM-41-SA).

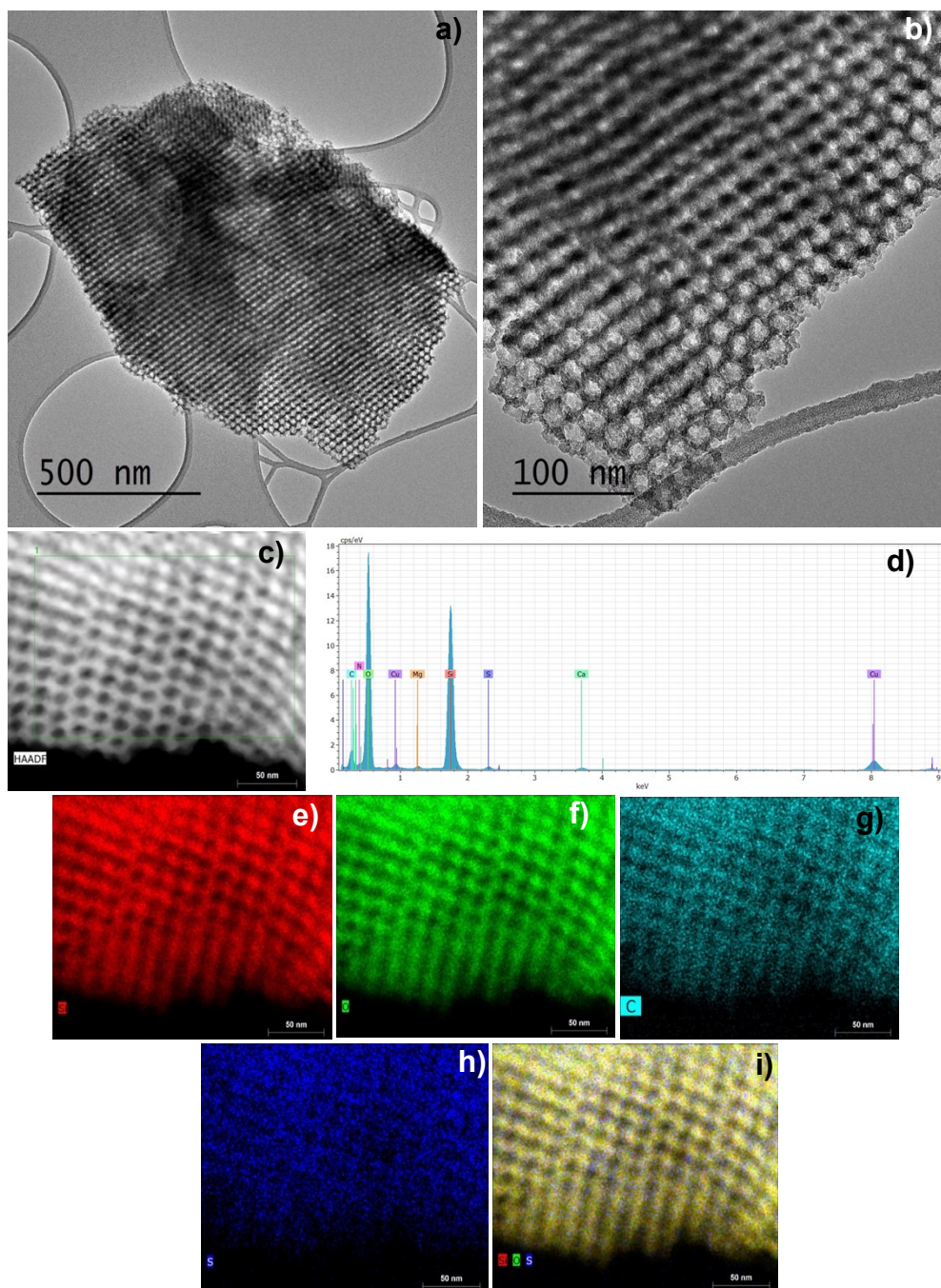


Figure S8. a) and b) HRTEM images, c) high-angle annular dark-field (HAADF) STEM image, d) EDS spectrum of the delimited area in Figure S2c and e) Si, f) O, g) C, h) S and i) Si, O and S elemental chemical mapping for the MCM-41-SA catalyst. Scale bar: a) 500 nm, b) 100 nm and c, e-i) 50 nm.

5.3 Morphological and elemental characterization of the sulfonated FDU-12 silica catalyst (FDU-12-SA).

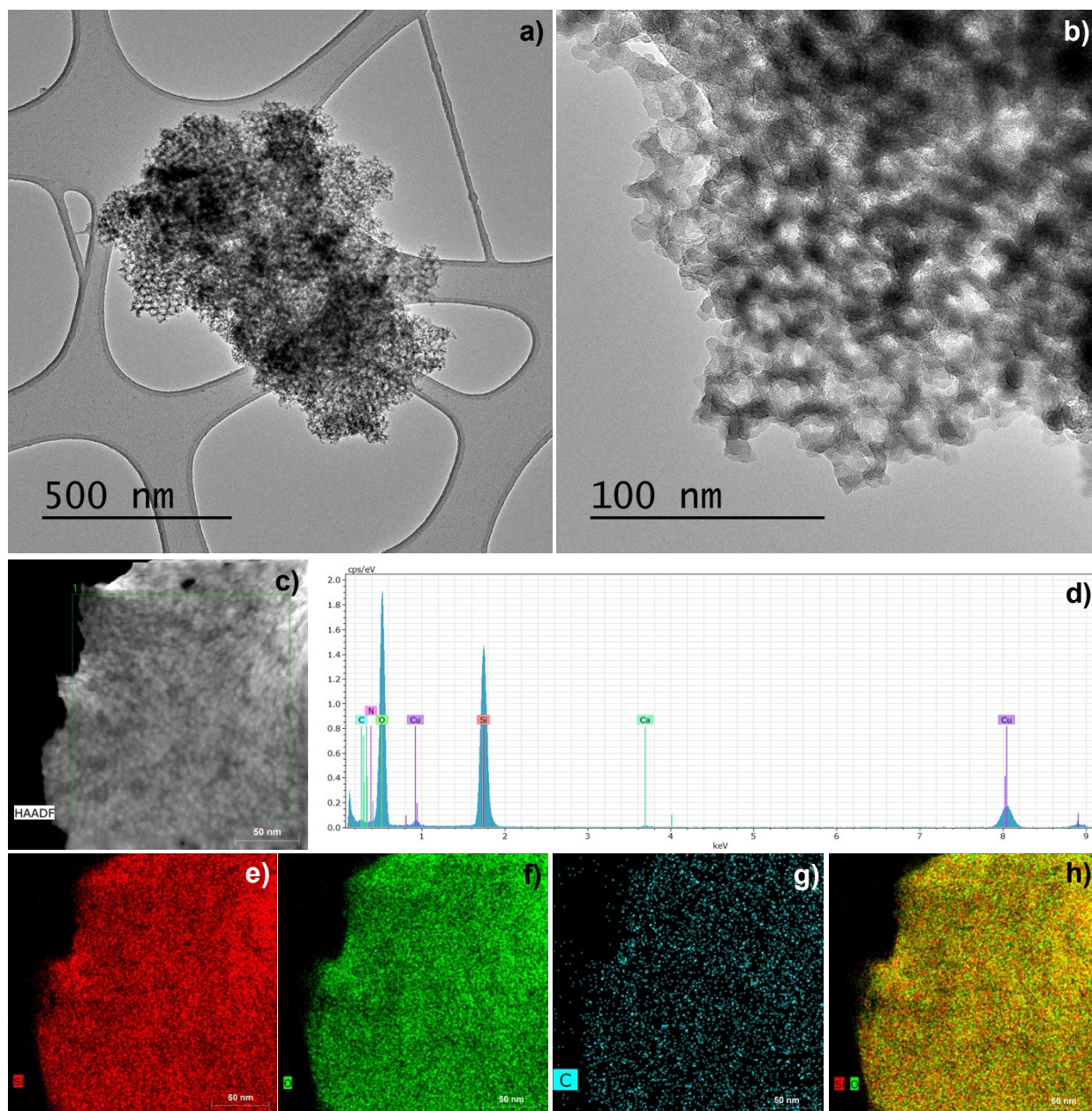


Figure S9. a) and b) HRTEM images, c) high-angle annular dark-field (HAADF) STEM image, d) EDS spectrum of the delimited area in Figure S3c and e) Si, f) O, g) C and h) Si, and O elemental chemical mapping for the FDU-12-SA catalyst. Scale bar: a) 500 nm, b) 100 nm and c, e-h) 50 nm.

5.4 Morphological and elemental characterization of the sulfonated Stöber silica catalyst (Stöber-SA).

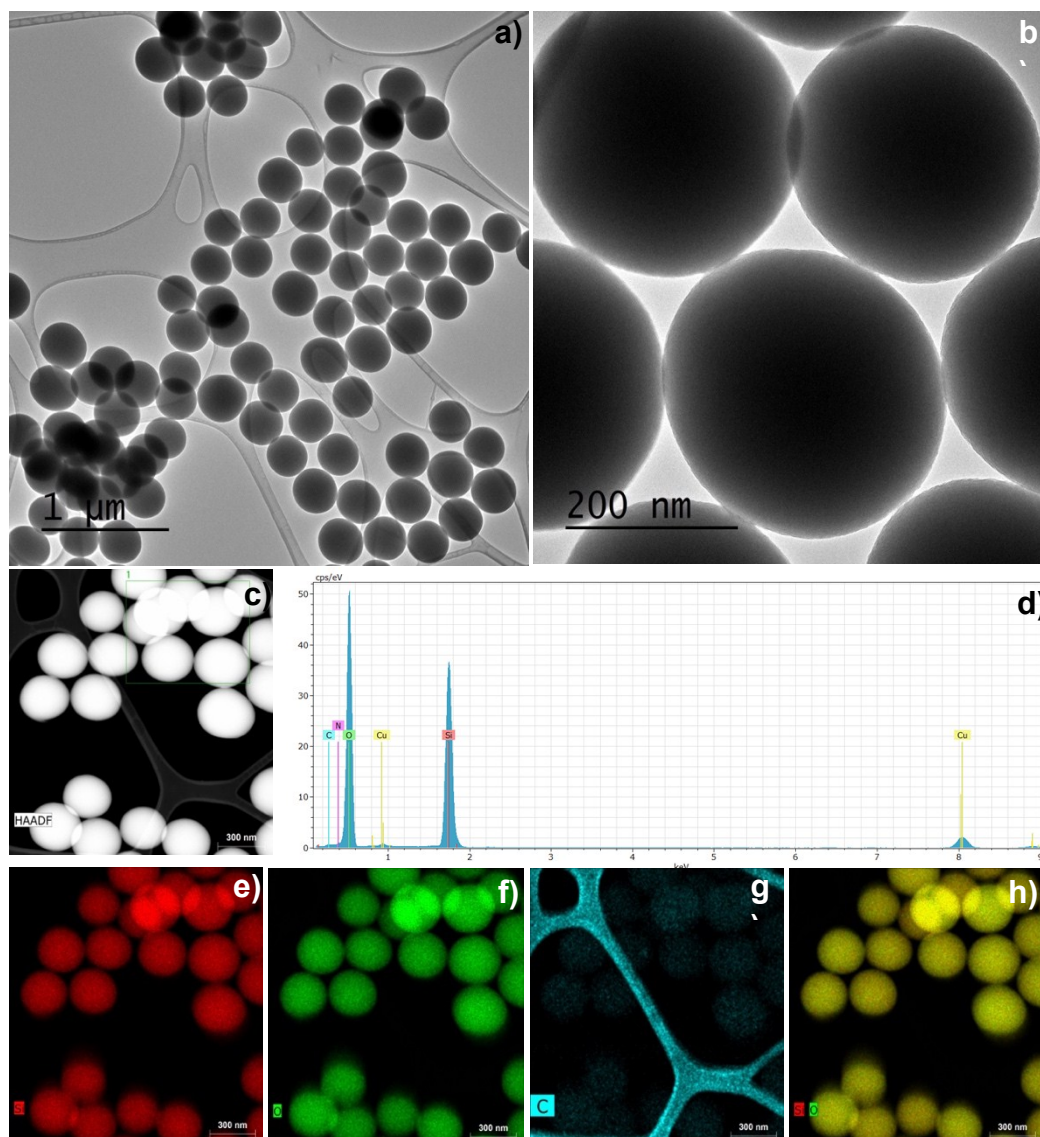


Figure S10. a) and b) HRTEM images, c) high-angle annular dark-field (HAADF) STEM image, d) EDS spectrum of the delimited area in Figure S4c and e) Si, f) O, g) C and h) Si, and O elemental chemical mapping for the Stöber-SA catalyst. Scale bar: a) 1 μm , b) 200 nm and c, e-h) 300 nm.

5.5 Morphological and elemental characterization of the sulfonated Silicalite-1 catalyst (Silicalite-1-SA).

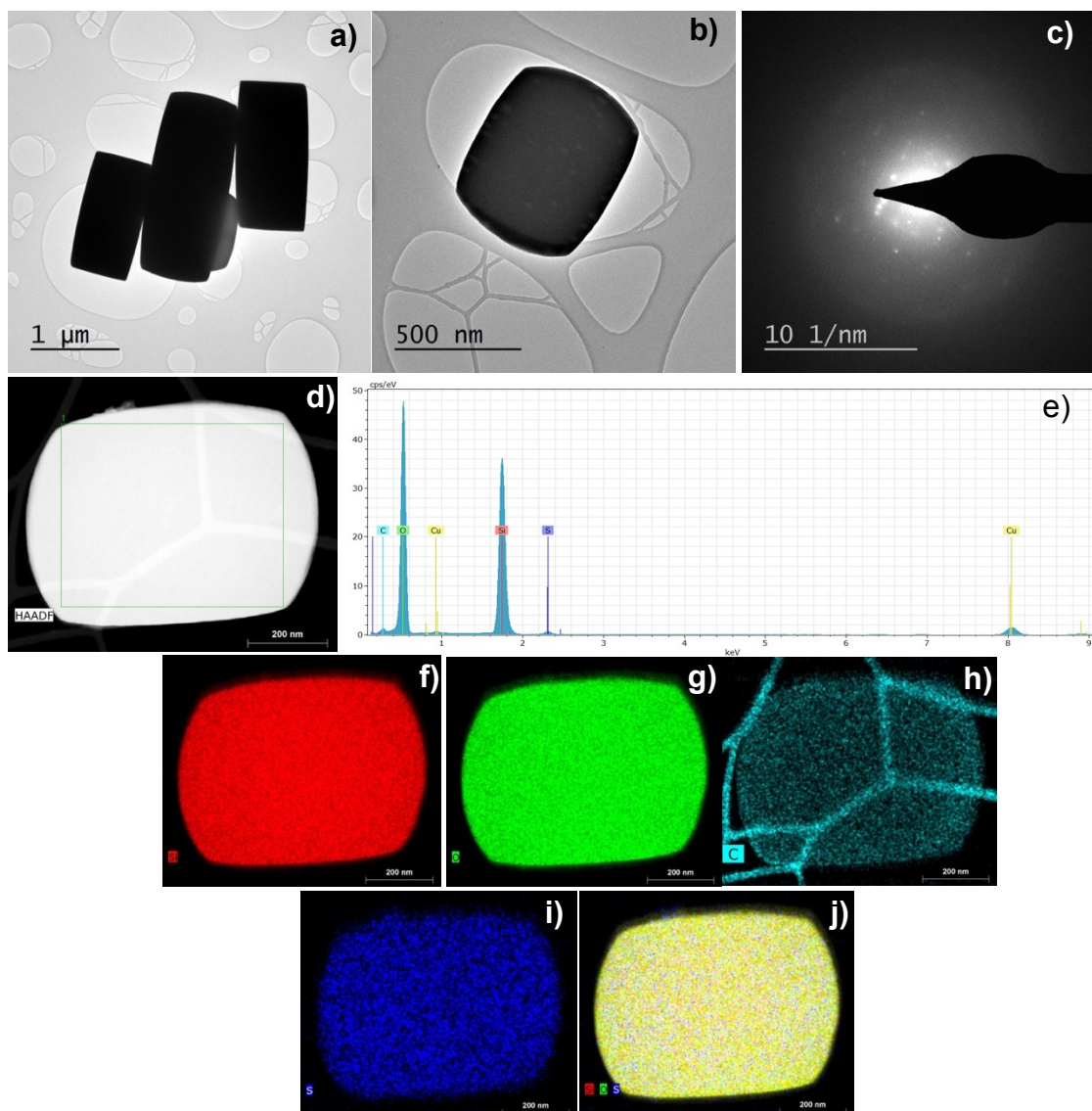


Figure S11. a) and b) HRTEM images, d) TEM diffraction pattern, d) high-angle annular dark-field (HAADF) STEM image, e) EDS spectrum of the delimited area in Figure S5d and f) Si, g) O, h) C, i) S and j) Si, O and S elemental chemical mapping for the Silicalite-1-SA catalyst. Scale bar: a) 1 μm , b) 500 nm and d, f-j) 200 nm.

5.6 Morphological and elemental characterization of the sulfonated SBA-15 silica catalyst (SBA-15-SA).

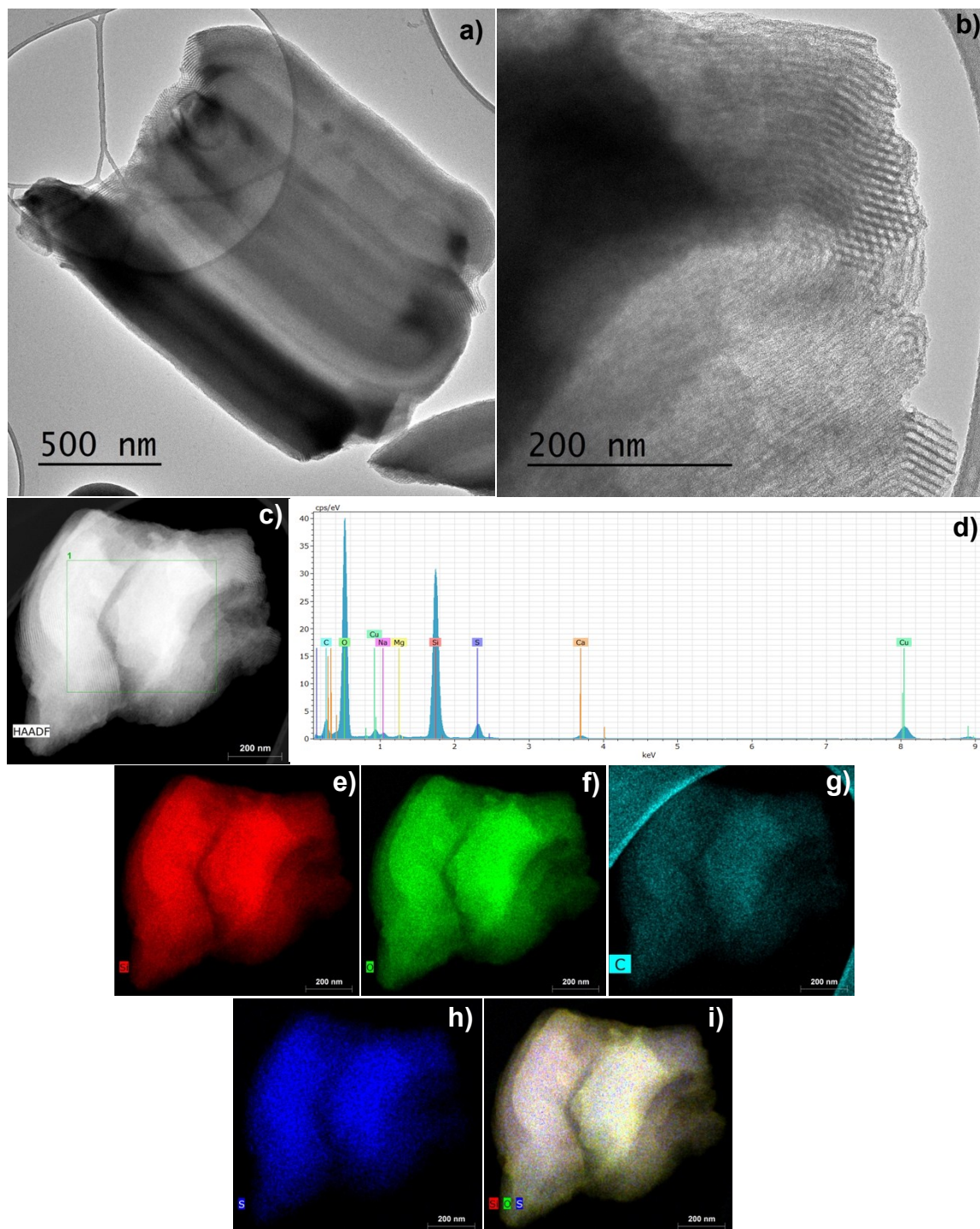


Figure S12. a) and b) HRTEM images, c) high-angle annular dark-field (HAADF) STEM image, d) EDS spectrum of the delimited area in Figure S6c and e) Si, f) O, g) C, h) S and i) Si, O and S elemental chemical mapping for the SBA-15-SA catalyst. Scale bar: a) 500 nm, b, c and e-i) 200 nm.

5.7 Morphological and elemental characterization of the sulfonated Flash silica catalyst (SBA-15-SA).

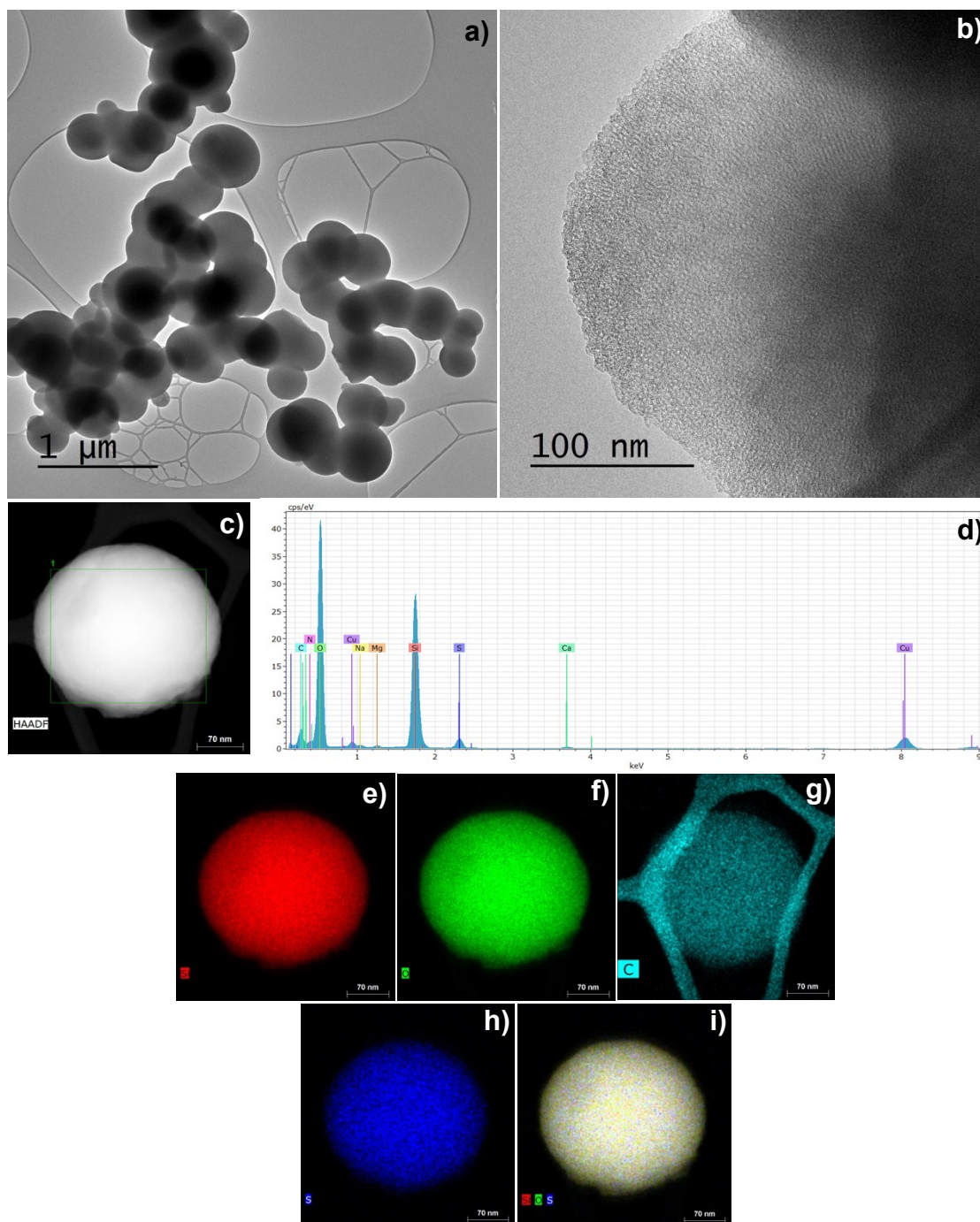


Figure S13. a) and b) HRTEM images, c) high-angle annular dark-field (HAADF) STEM image, d) EDS spectrum of the delimited area in Figure S7c and e) Si, f) O, g) C, h) S and i) Si, O and S elemental chemical mapping for the Flash-SA catalyst. Scale bar: a) 1 μm , b) 100 nm, c and e-i) 70 nm.

5.8 Textural characterization of the KCC-1 silica support and the KCC-1-SA catalyst.

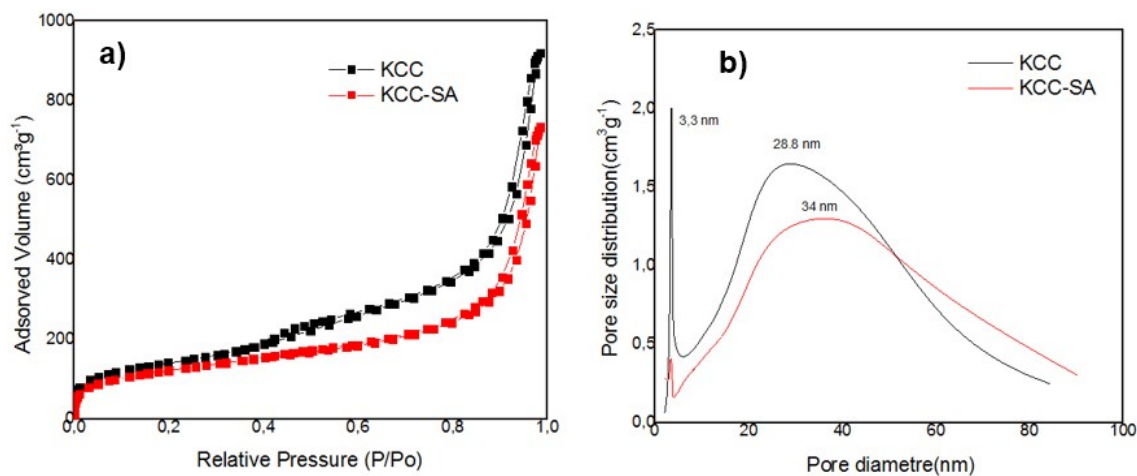


Figure S14. a) Isotherms of adsorption/desorption of N₂ and b) pore distribution for KCC-1 and KCC-1-SA.

5.9 Textural characterization of the MCM-41 silica support and the MCM-41-SA catalyst.

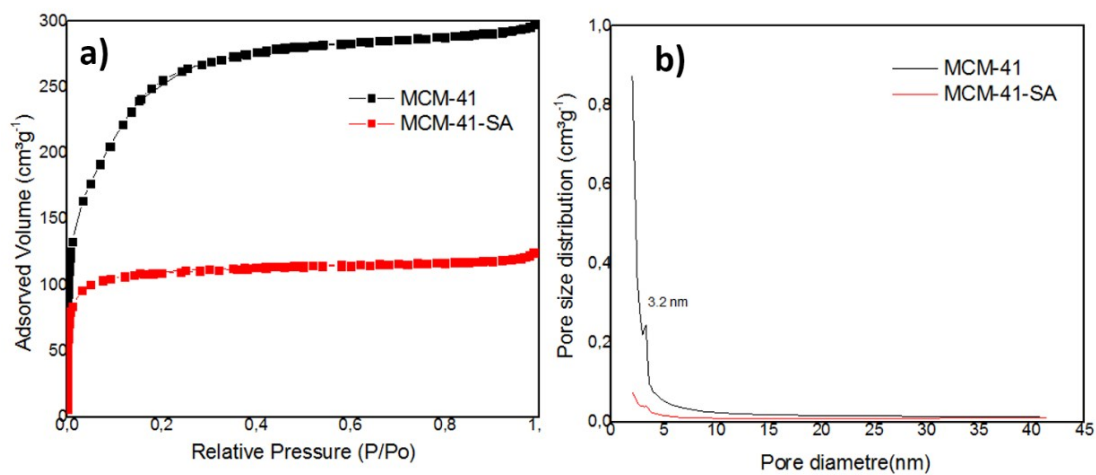


Figure S15. a) Isotherms of adsorption/desorption of N₂ and b) pore distribution for MCM-41 and MCM-41-SA.

5.10 Textural characterization of the FDU-12 silica support and the FDU-12-SA catalyst.

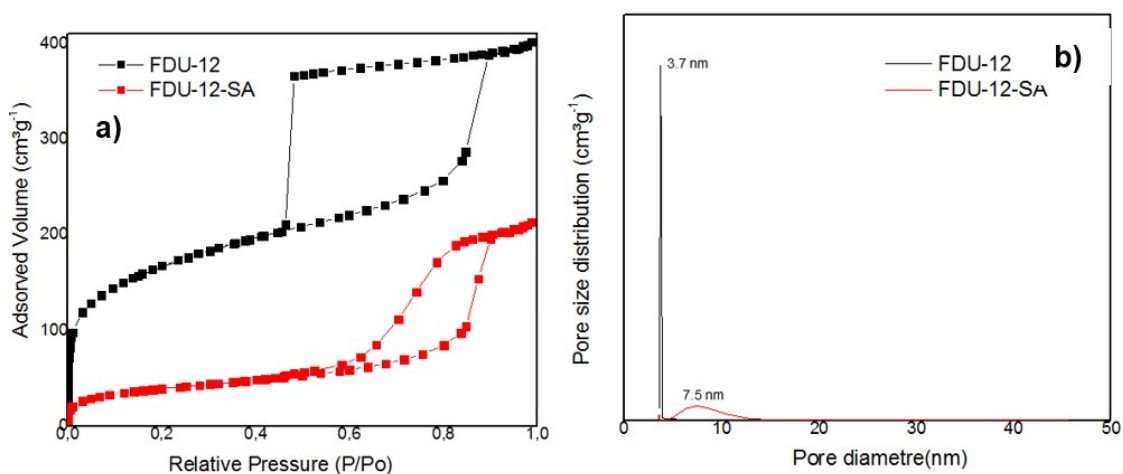


Figure S16. a) Isotherms of adsorption/desorption of N₂ and b) pore distribution for FDU-12 and FDU-12-SA.

5.11 Textural characterization of the Stöber silica support and the Stöber-SA catalyst.

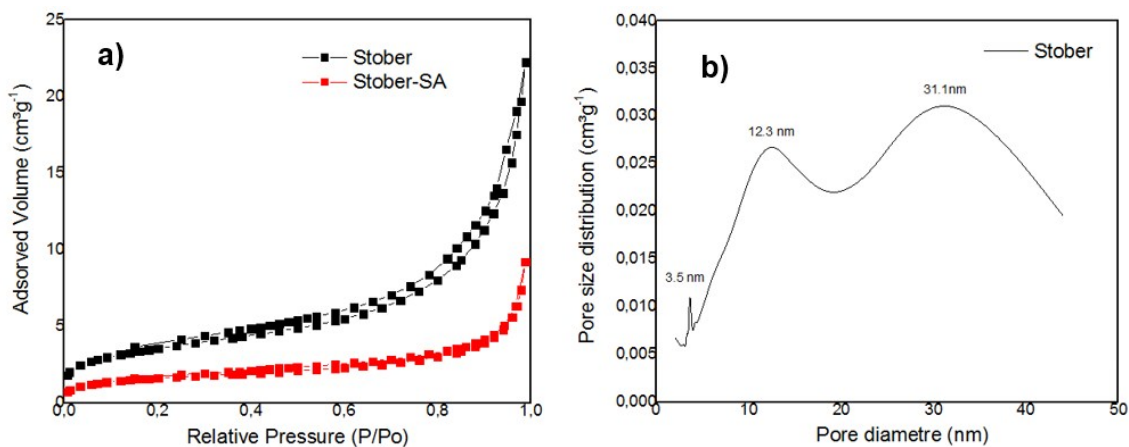


Figure S17. a) Isotherms of adsorption/desorption of N₂ and b) pore distribution for the Stöber silica and Stöber-SA.

5.12 Textural characterization of the Silicalite-1 support and the Silicalite-1-SA catalyst.

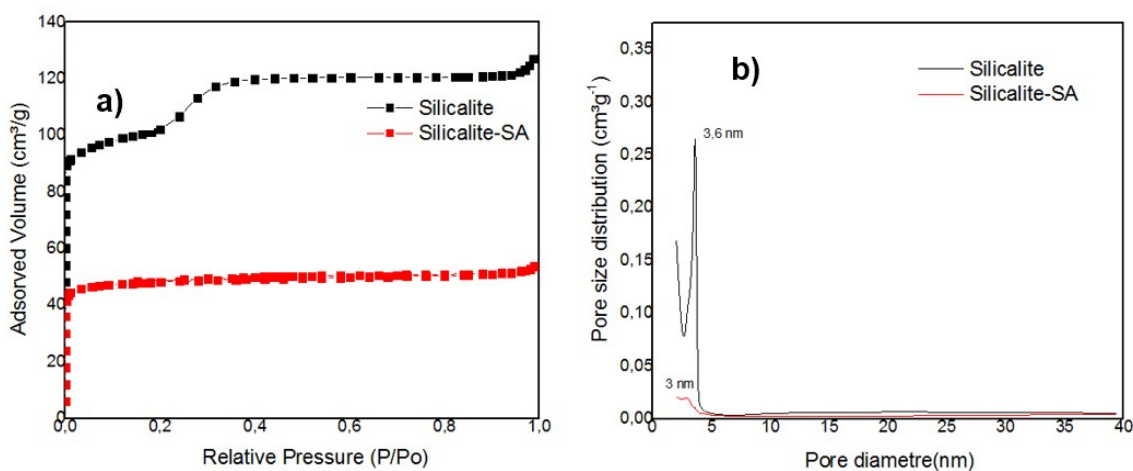


Figure S18. a) Isotherms of adsorption/desorption of N₂ and b) pore distribution for the Silicalite-1 and Silicalite-1-SA.

5.13 Textural characterization of the SBA-15 silica support and the SBA-15-SA catalyst.

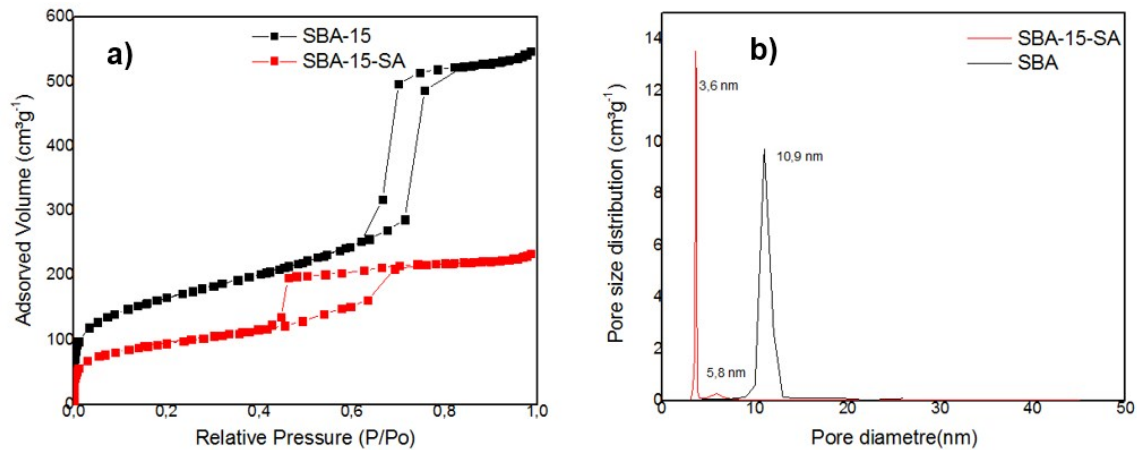


Figure S19. a) Isotherms of adsorption/desorption of N₂ and b) pore distribution for the SBA-15 silica and SBA-15-SA.

5.14 Textural characterization of the Flash silica support and the Flash-SA catalyst.

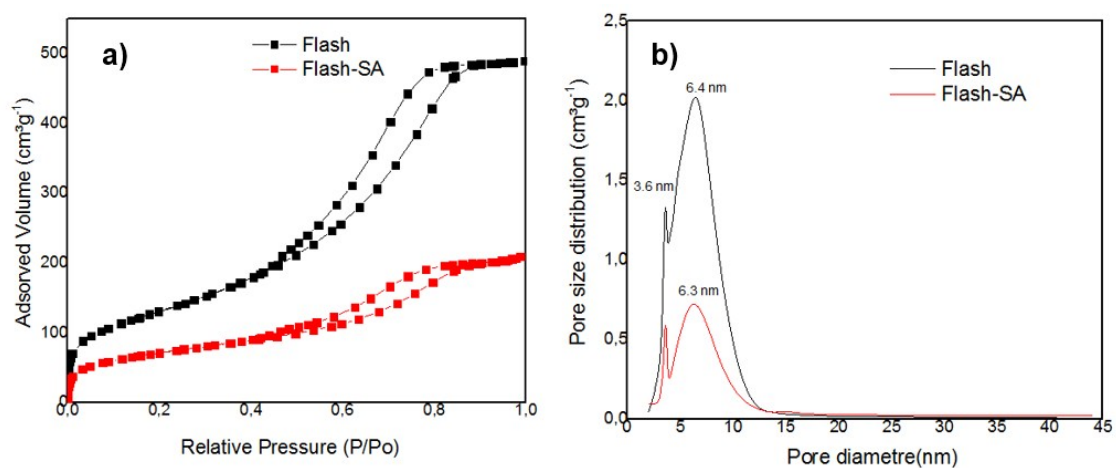


Figure S20. a) Isotherms of adsorption/desorption of N₂ and b) pore distribution for the Flash silica and Flash-SA.

Table S1. Textural characterization data for the silica supports and catalysts.

Sample	B.E.T. Surface Area (m ² g ⁻¹)	Microp. area (m ² g ⁻¹) ^a	Total pore volume (cm ³ g ⁻¹) ^b	Microp. volume (cm ³ g ⁻¹) ^a	Pore diameter (nm) ^b	Pore size dist. (nm)	Isotherm type	Hysteresis type
SBA-15	578.8	105.2	0.782	0.0491	6.4	6.5	IV	H1
SBA-15-SA	327.7	74.1	0.336	0.0354	4.0	3.6	IV	H2
DMSi	704.7	50.8	1.711	0.0199	11.4	3.5; 6.4; 25.9	IV	H3
DMSi-SA	286.2	20.3	0.768	0.00765	11.5	3.7; 5.6; 25.2	IV	H3
MCM-41	877.3	---	0.178	---	2.5	2.7	IV	n.d.
MCM-41-SA	345.3	---	0.0309	---	3.7	3.4	IV	n.d.
FDU-12	580.9	---	0.589	---	3.9	3.8	IV	H2
FDU-12-SA	138.1	---	0.328	---	7.8	3.6; 6,9	IV	H2
Stöber	12.6	---	0.0278	---	10.3	4.0; 10.5; 31.0	II	---
Stöber-SA	5.7	---	0.00871	---	8.6	3.7; 5.4; 14,0	II	---
KCC-1	505.1	41.6	1.399	0.0166	10.8	3.6; 23.0	IV	H1
KCC-1-SA	439.0	19.9	1.069	0.00569	12.4	3.9; 6.4; 25.4	IV	H1
Flash	479.7	---	0.773	---	5.3	3.7; 5.9	IV	H2
Flash-SA	253.1	---	0.299	---	5.2	3.6; 6.4	IV	H2
Silicalite-1	291.7	186.6	0.0407	0.0929	3.6	1.9; 3.8	I	---
Silicalite-1-SA	150.4	132.4	0.0107	0.0667	3.5	2.7	I	---

^aCalculated using t-plot method, ^bCalculated using B.J.H. method, ^{n.d.}Hysteresis loop was not observed.

5.15 Characterization of the oxidation state of the sulfur species in the samples using X-ray photoelectron spectroscopy (XPS)

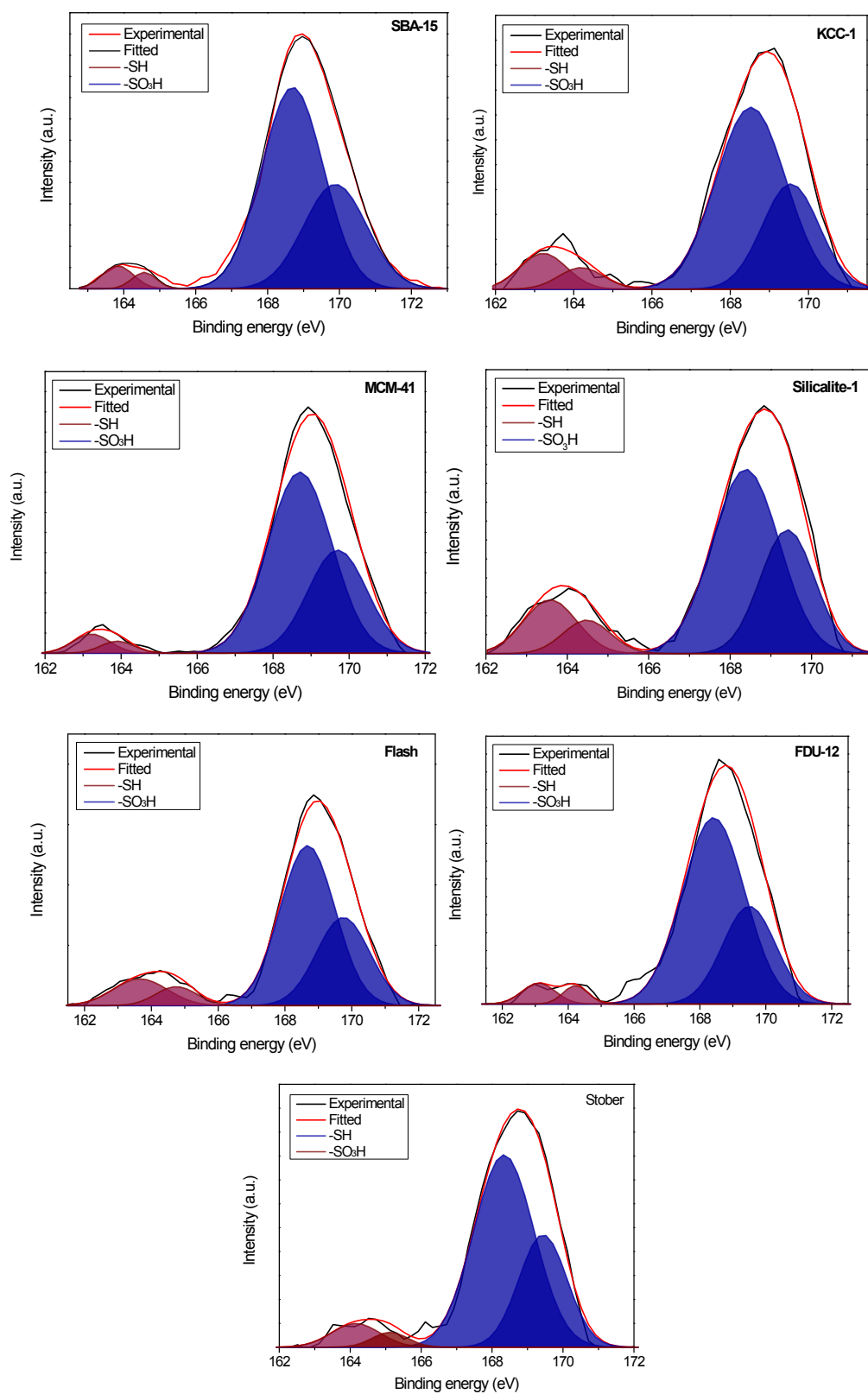


Figure S21. XPS spectra for the sulfonic-acid functionalized silica catalysts.

Table S2. Parameters extracted from the XPS spectra of the sulfonic-acid functionalized silica catalysts depicted in Figure S15.

Sample	Area S2p _{3/2}	Area S2p _{1/2}	Total - SH (%)	Area S2p _{3/2}	Area S2p _{1/2}	Total - SO ₃ H (%)
SBA-15	29.4	16.5	5.5	510.5	270.39	94.5
MCM-41	29.1	16.3	5.9	477.0	250.3	94.1
KCC-1	21.7	12.4	12.4	163.6	77.0	87.6
Silicalite-1	46.6	25.8	18.9	200.6	109.9	81.1
Flash	44.9	24.2	14.1	273.9	145.7	85.9
FDU-12	14.8	9.8	6.3	240.2	120.2	93.7
Stöber	16.9	7.85	8.9	171.8	80.2	91.1

5.16 Characterization of type of acid sites present in the samples using Fourier-transform infrared of adsorbed pyridine (Pyr-FTIR)

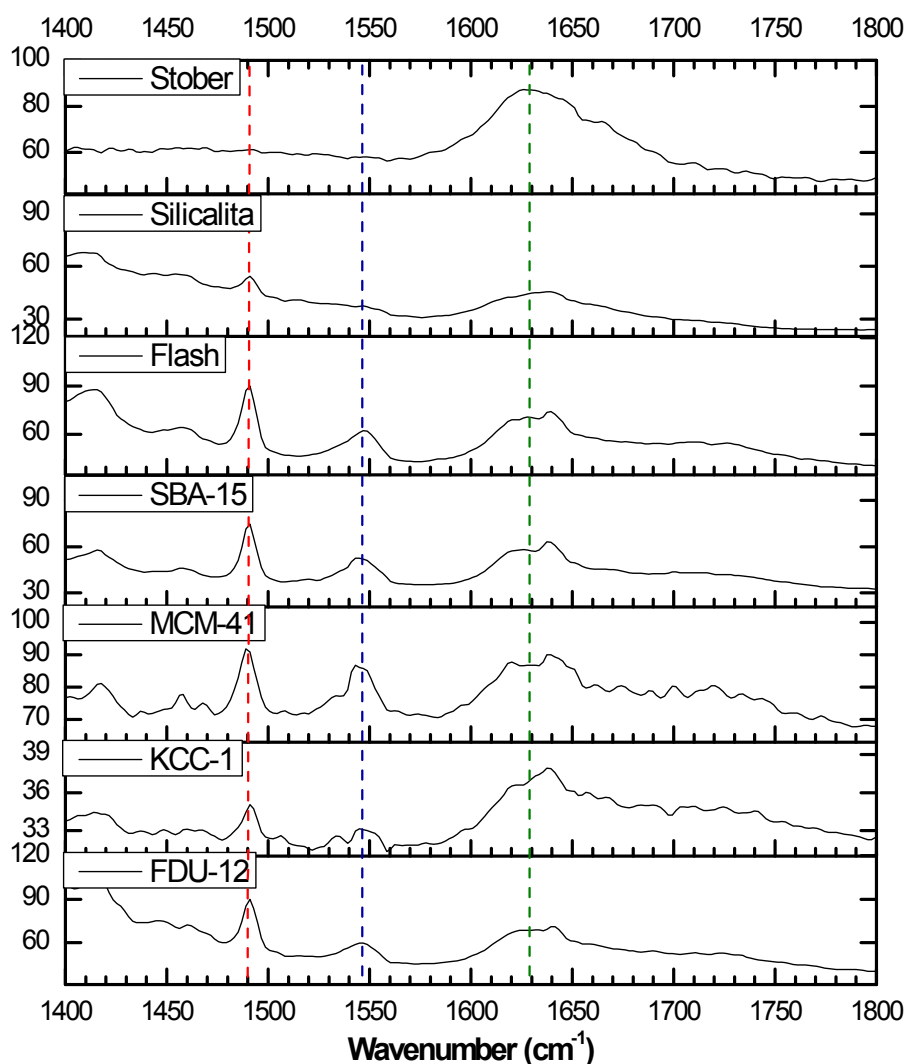


Figure S22. Fourier transform infrared spectra of adsorbed pyridine for the sulfonic-acid functionalized silica catalysts.

6. Discussion on the characterization and catalytic evaluation of different sulfonic acid-functionalized silica materials

Initially, the textural characterization of the silica supports as well as the final catalysts were conducted by nitrogen physisorption (Table S1). As expected, following the DMSi trend, all of the textural properties of the silica supports showed a significant change after the functionalization with sulfonic acid groups. Additionally, when compared to the total sulfur content showed in Table S1, it is noticed that the silica materials (MCM-41, DMSi, and KCC-1) with the highest surface area underwent a higher degree of functionalization. Interestingly, commercially flash silica also showed a high degree of functionalization, and although it has a considerably lower surface area when compared to MCM-41, for instance, flash silica has a significantly higher value of pore size and volume.

The HRTEM-EDS and chemical mapping confirmed the presence of silicon, oxygen and sulfur atoms in the sulfonic acid-functionalized silica materials, with a homogeneous distribution of the sulfur atoms throughout the structure (Figures S6-12). On the other hand, in the case of the Stöber-SA, the HRTEM-EDS confirmed the presence of silicon and oxygen, but no sulfur, indicating that the functionalization of the material has not occurred or to a very low extent, below the limit of the equipment's detection limit (Figure S9d).

In this context, in order to determine the oxidation state of the sulfur species in the samples, XPS analyses were performed (Figure S20 and Table S2). The results showed that similarly to DMSi-SA, the sulfur species are present in the form of two species, -SH and -SO₃H, with varying ratios depending on the silica materials, with DMSi-SA showing the highest amount of thiol groups among all silica materials. The total amount of sulfur was quantified by ICP-OES, and the total acidity of the samples was determined by aqueous titration (Table S3). Overall, the results obtained by XPS have a good correspondence with the ones obtained by titration; the acidity value obtained for Stöber-SA, for instance, was 0.04 mmol·g⁻¹, which explains why sulfur could not be observed in the EDS and elemental mapping analysis.

Table S3. Chemical properties of the sulfonic acid-functionalized silica samples.

Silica-SA	-SH^a (%)	-SO₃H^a (%)	Total sulfur content ^b (mmol/g)	-SO₃H^c (mmol/g)	ρ_{acidsite}^d (mmol/m²)
MCM-41	5.9	94.1	1.58	1.46	0.0042
KCC-1	12.4	87.6	1.03	0.96	0.0022
Silicalite-1	18.9	81.1	0.49	0.12	0.0067
Flash	14.1	89.5	1.41	1.48	0.0058
FDU-12	6.3	93.7	0.95	1	0.0072
Stöber	8.9	91.1	0.04	0.032	0.0046
SBA-15	5.5	94.5	1.75	1.82	0.0056

^aDetermined by XPS, ^bDetermined by ICP-OES, ^cDetermined by aqueous titration, ^dNumber of acid sites/total surface area.

Finally, in order to determine the nature of the acidic sites present in the samples, infrared analyses of absorbed pyridine were performed (Figure S21). The results show that most of the samples present bands around 1630 cm⁻¹ and 1550 cm⁻¹, characteristic of Brønsted acid sites, and a band around 1490 cm⁻¹ which can be ascribed to Brønsted and Lewis acid sites; in the case of Stöber-SA, only the band at 1630 cm⁻¹ was noticeable.

7. Additional chromatographic data used for the quantification of the products

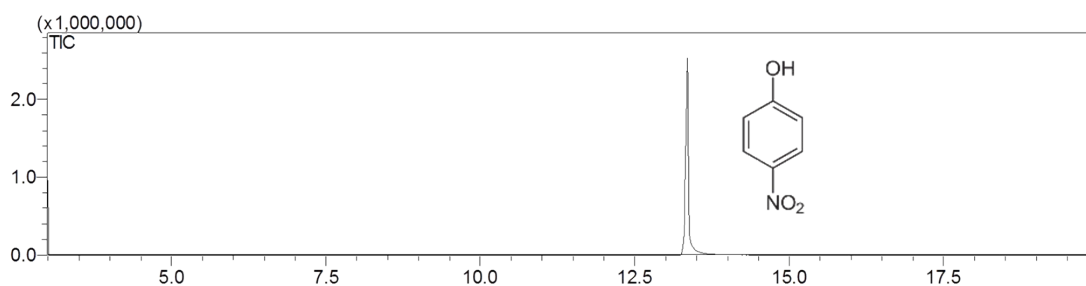


Figure S23. GC-MS chromatogram of the internal standard *p*-nitrophenol.

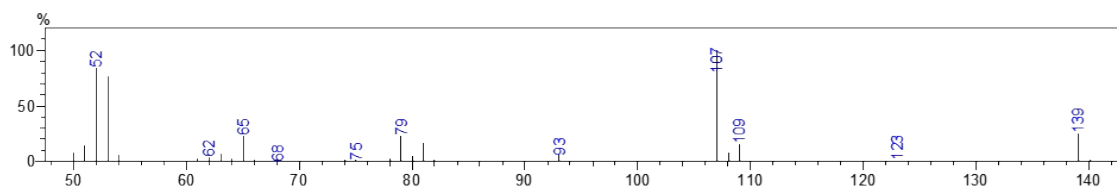


Figure S24. Mass spectrum of the peak assigned to the internal standard *p*-nitrophenol in the chromatogram showed in Figure S22.

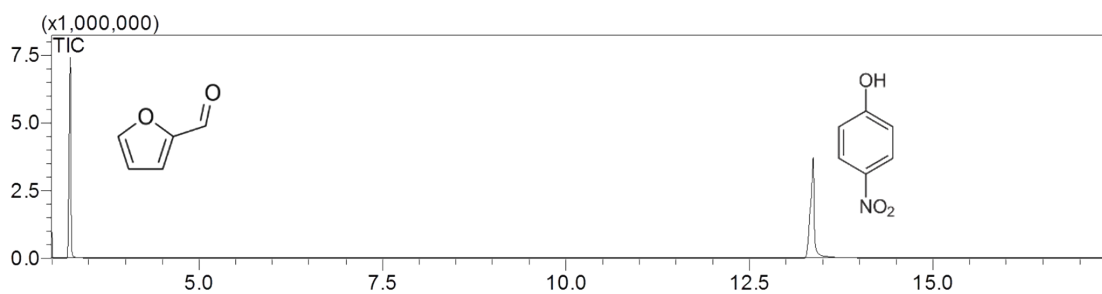


Figure S25. GC-MS chromatogram of the furfural standard in the presence of the internal standard *p*-nitrophenol.

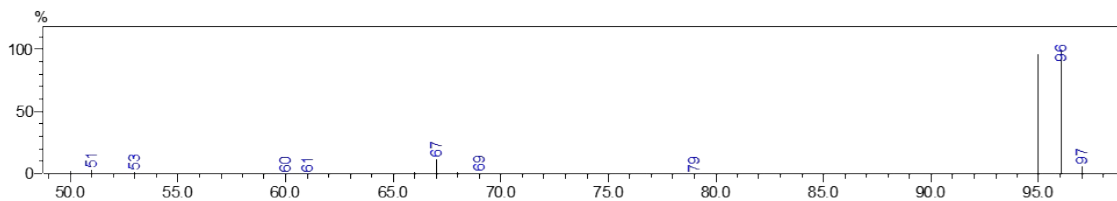


Figure S26. Mass spectrum of the peak assigned to furfural in the chromatogram showed in Figure S24.

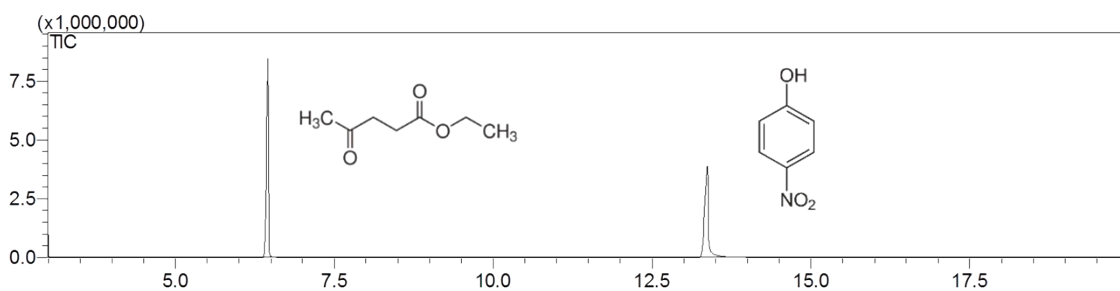


Figure S27. GC-MS chromatogram of the ethyl levulinate standard in the presence of the internal standard *p*-nitrophenol.

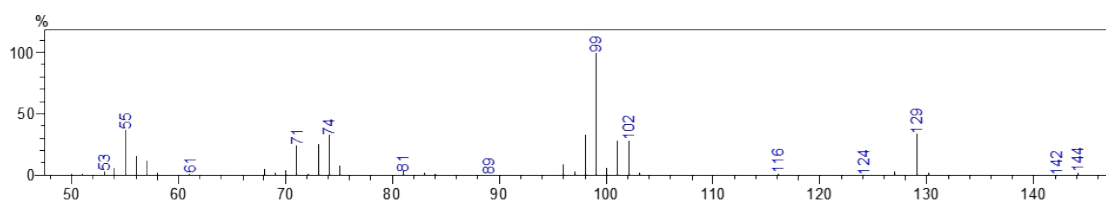


Figure S28. Mass spectrum of the peak assigned to ethyl levulinate in the chromatogram showed in Figure S26.

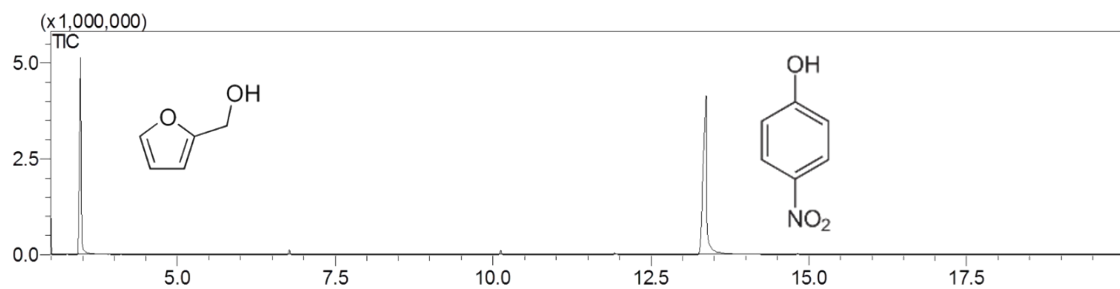


Figure S29. GC-MS chromatogram of the furfuryl alcohol standard in the presence of the internal standard *p*-nitrophenol.

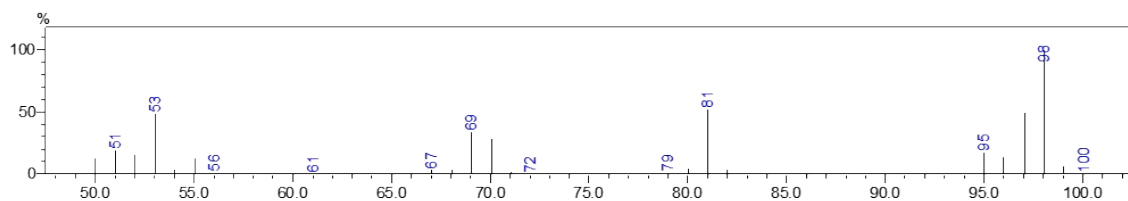


Figure S30. Mass spectrum of the peak assigned to furfuryl alcohol in the chromatogram showed in Figure S28.

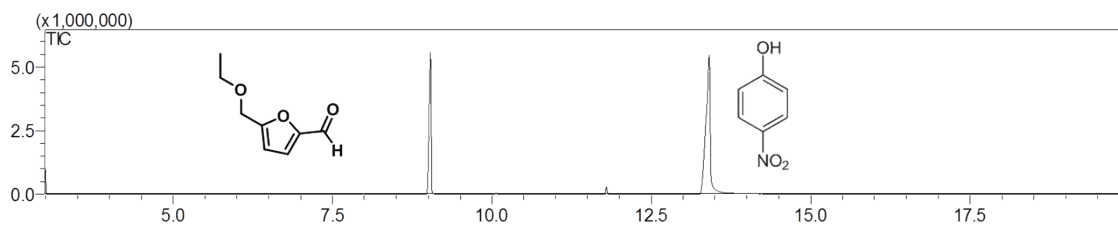


Figure S31. GC-MS chromatogram of the 5-(ethoxymethyl)furfural (EMF) standard in the presence of the internal standard *p*-nitrophenol.

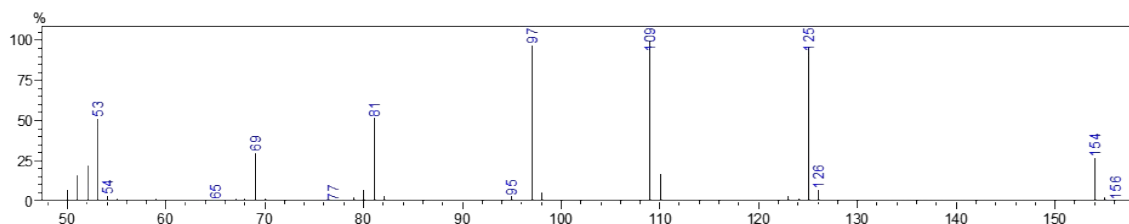


Figure S32. Mass spectrum of the peak assigned to EMF in the chromatogram showed in Figure S30.

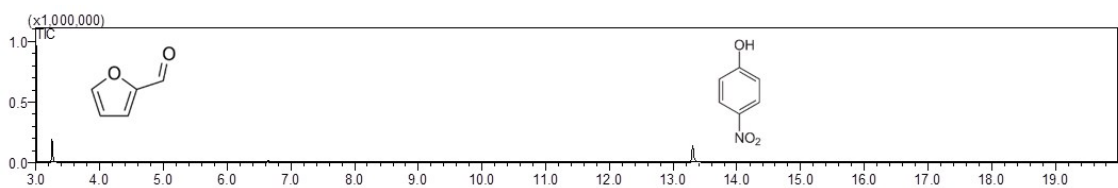


Figure S33. GC-MS chromatogram of the reaction mixture after the dehydration of D-xylose to furfural using the DMSi-SA catalyst under optimized conditions.

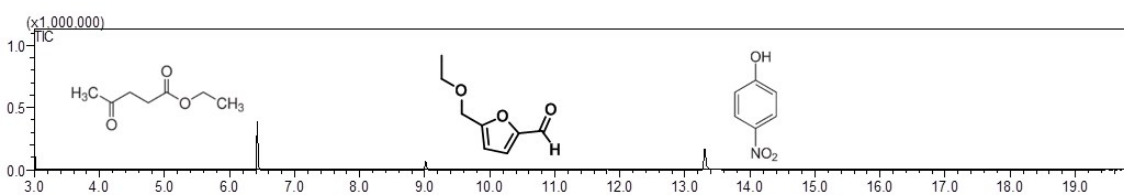


Figure S34. GC-MS chromatogram of the reaction mixture after the conversion of D-fructose to ethyl levulinate using the DMSi-SA catalyst under optimized conditions.

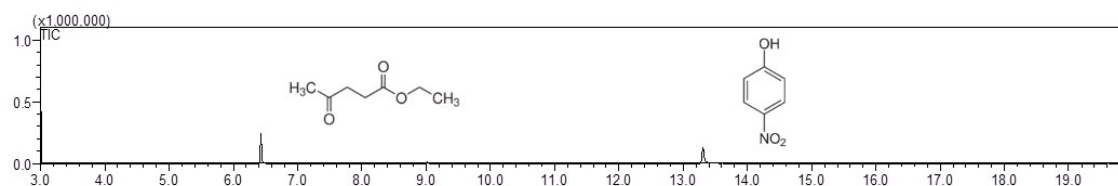


Figure S35. GC-MS chromatogram of the reaction mixture after the conversion of D-glucose to ethyl levulinate using the DMSi-SA catalyst under optimized conditions.

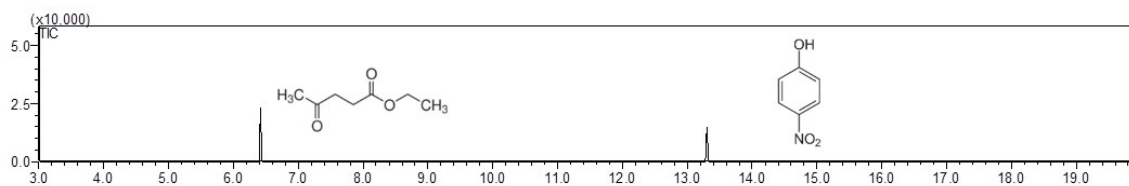


Figure S36. GC-MS chromatogram of the reaction mixture after the conversion of sucrose to ethyl levulinate using the DMSi-SA catalyst under optimized conditions.

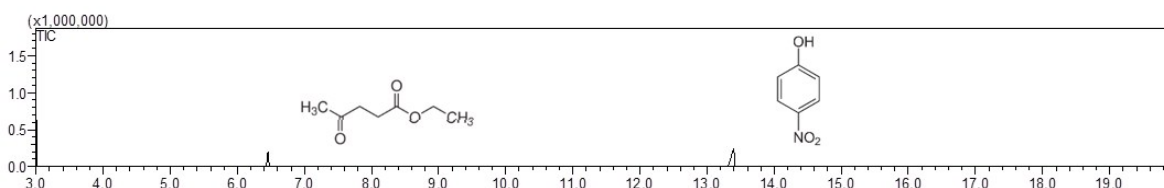


Figure S37. GC-MS chromatogram of the reaction mixture after the conversion of cellulose to ethyl levulinate using the DMSi-SA catalyst in the best observed conditions.

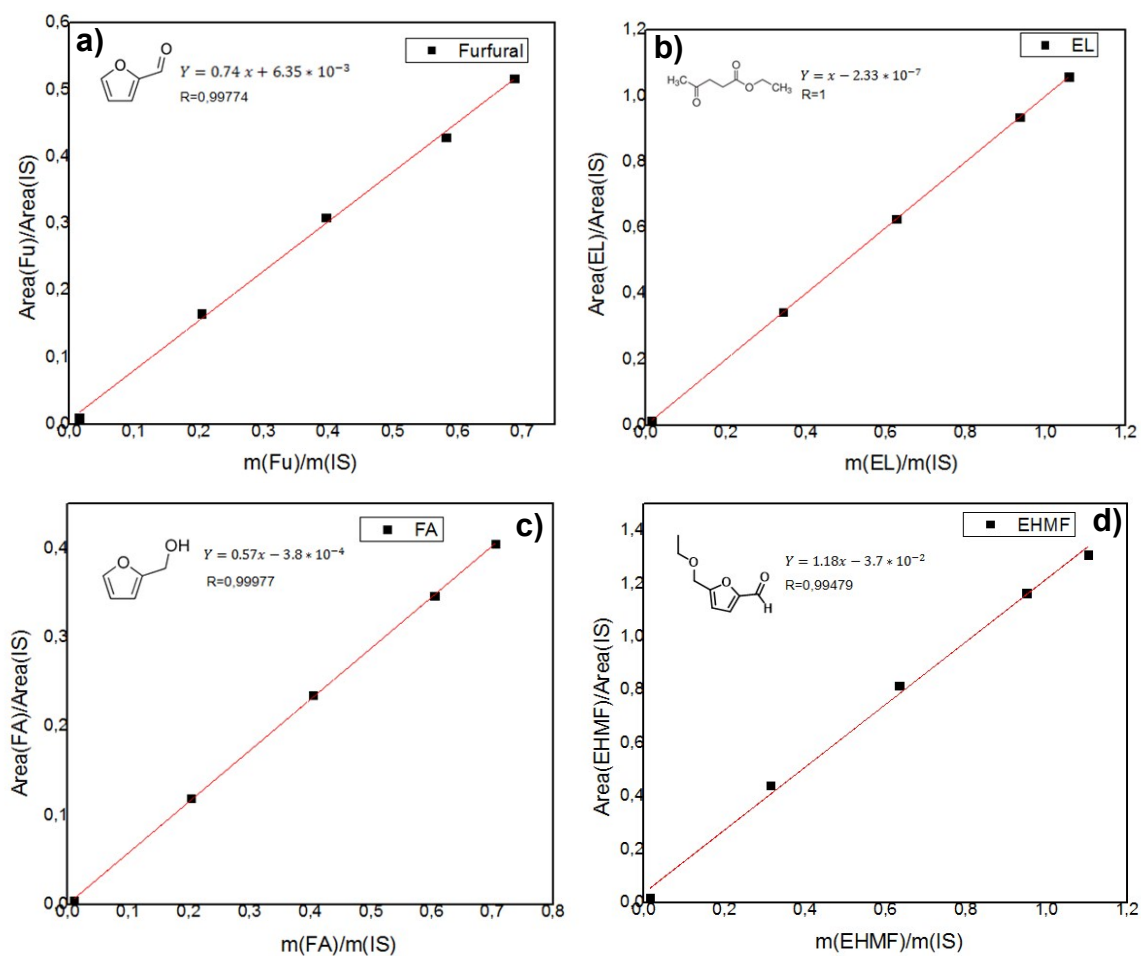


Figure S38. Calibration curves obtained for the standards a) furfural, b) ethyl levulinate, c) furfuryl alcohol and d) EMF in the presence of the internal standard *p*-nitrophenol.

8. References

- [1] D. Zhao, Q. Huo, J. Feng, B. F. Chmelka and G. D. Stucky, *J. Am. Chem. Soc.* 1998, **124**, 6024-6036.
- [2] M. Grün, K. Unger, A. Matsumoto and K. Tsutsumi, *Micropor. Mesopor. Mater.* 1999, **27**, 207-216.
- [3] M. Kruk and C. M. Hui, *Micropor. Mesopor. Mater.* 2008, **14**, 64-73.
- [4] X.-D. Wang, Z.-X. Shen, T. Sang, X.-B. Cheng, M.-F. Li, L.-Y. Chen and Z.-S. Wang, *J. Colloid Interf. Sci.* 2010, **341**, 23-29.
- [5] M. Zhou, A. A. Rownaghi and J. Hedlund, *RSC Adv.* 2013, **3**, 15596-15599.
- [6] C. Pirez, A. F. Lee, J.C. Manayil, C. M. A. Parlett and K. Wilson, *Green Chem.* 2014, **16**, 4506-4509.
- [7] E. Cano-Serrano, G. Blanco-Brieva, J. M. Campos-Martin and J. L. G. Fierro, *Langmuir* 2003, **19**, 7621-7627.